RSC Advances

ROYAL SOCIETY OF CHEMISTRY

www.rsc.org/advances

Bismuth oxide nanoparticle as a nanoscale guide to form silver-polydopamine hybrid electrocatalyst with enhanced activity and stability for oxygen reduction reaction

Settu Murali, Jen-Lin Chang and Jyh-Myng Zen*

Department of Chemistry, National Chung Hsing University, Taichung 40227, Taiwan.

E-mail: jmzen@dragon.nchu.edu.tw, Tel/Fax: +886 4 22850864, +886 4 22854007.

† Electronic supplementary information (ESI) available. See DOI:

High dispersion Ag nanoparticles (Ag NPs) were successfully synthesized on functionalized polydopamine (PDA)@Bi_2O_3 NPs for use as electrocatalyst. In the proposed method, a uniform layer of PDA was first coated on Bi_2O_3 NPs. The surface of the PDA@Bi_2O_3 can then be used as a nanoscale guide to deposit Ag NPs and hence the formation of Ag-PDA@Bi_2O_3 hybrid nanocatalysts. It was found that Ag NPs enhanced the electrocatalytic ability on PDA@Bi_2O_3 by synergetic effect for direct $4e^-$ transfer in oxygen reduction reaction (ORR) with a low overpotential. The surface morphology and lattice fringes of Ag NPs crystalline nature of the obtained Ag-PDA@Bi_2O_3 hybrid nanocatalysts were examined through HR-TEM and SAED pattern. The material's purity and chemical functional groups were identified by FT-IR analysis. This strategy provides new opportunities to design and optimize heterogeneous nanocatalysts with tailored size, morphology, chemical configuration and supporting substrates for metal-catalyzed reactions.

Introduction

We report here the application of polydopamine (PDA) coating-directed substrate-immobilization of Ag nanoparticles (Ag NPs) as a promising material in oxygen reduction reaction (ORR). Note that ORR is essential in various applications, such as fuel cells , metal-air batteries, catalysis, enzymatic reactions and estimation of dissolved oxygen in bio/environment samples.[1–6] Recent efforts in ORR electrocatalysis have focused on improving the catalytic activity of Pt alloys, minimizing Pt content by utilizing a core-shell structure, preparing Pt supporting material via synergetic effect and replacing Pt with less expensive materials.[1,7,8] For example, several materials, such as Co,[1,9] metal oxides/composites,[1,3,4] Ag,[10–18] and N, S, B, P–doped carbon based materials,[19–25] were reported to replace Pt for ORR.

Since PDA layer can be formed easily on the surface of Bi_2O_3 NPs, our strategy is to use the PDA@Bi_2O_3 as a nanoscale guide to form uniform Ag NPs on the surface of PDA@Bi_2O_3. Silver can be regarded as a less-expensive and relatively abundant metal, exhibits good ORR activity in alkaline media,[15,16] especially for HO_2^- disproportionation.[17,18] In addition, N-containing compounds and polymers were reported to prepare ORR catalyst for tuning the metal nanoparticle size, surface area, complex formation, hetero atom doping with higher stability and durability.[1,2,19,20] Synergetic effects of within metal, metal oxide, carbon nano-materials, mixed composites material, *etc.* were demonstrated to increase the catalytic activity. Of course, the main advantage of PDA is that it could be easily self-polymerized in basic pH medium on any matrix surfaces with multiple applications in variety of fields.[26] It has shown good adhesive and reducing properties with higher amount

of nanoparticle loading and different structure nanomaterial formation.[27] Meanwhile, both PDA–based materials and bismuth-combined composites have also shown enhanced activity in ORR.[9,28–33]

Herein, an easily modified large surface area Non Hazardous Nano Composite (NHNC) material based on Ag–PDA@Bi_2O_3 was demonstrated to have enhanced catalytic behavior towards ORR. A key issue for ORR activity at Ag or other catalysts is whether O_2 is reduced by two electrons to H_2O_2 (or HO_2^-) or four electrons to water (or OH^-), i.e., with an n-value of 2 or 4. In general, an n-value of 4 is the preferred pathway, because of both the higher currents available and the unwanted chemical reactivity of H_2O_2 and its decomposition products toward various fuel cell components. In this paper, we thoroughly studied the electrocatalytic ability of the Ag–PDA@Bi_2O_3 for direct $4e^-$ transfer in ORR with a low overpotential. The surface morphology, lattice fringes and crystal plane of the obtained Ag–PDA@Bi_2O_3 hybrid nanocatalysts were examined through HR-TEM and SAED pattern..

Experimental

Dopamine hydrochloride was received from Sigma Aldrich. Sodium dihydrogen phosphate, disodium hydrogen phosphates were purchased from SHOWA chemicals, Japan. Silver nitrate ($AgNO_3$), Tris-HCl, nano MnO_2 and Bismuth oxide were of ACS grade chemicals. The disposable Screen Printed Carbon Electrode (SPCE) (geometrical area 0.2 cm^2) and Ring Disk SPCE (RDSPCE) were purchased from Zensor R&D laboratory, Taichung, Taiwan.

Millipore deionized water (18 MΩ cm^{-1}) was used for throughout this experiments. All chemicals were used without further purifications.

To prepare the PDA@Bi_2O_3 composite, 100 mg Bi_2O_3 was dispersed in 100 mL of Tris-HCl (10 mM) under ultra-sonication for 10 min. Then, 200 mg dopamine–HCl was introduced into the solution and allowed to continuous stirring for 12 h. The obtained precipitate was centrifuged, washed with distilled water and dried at 60 °C. As to the preparation of Ag-PDA@Bi_2O_3 composite, 5 mg of PDA@Bi_2O_3 composite was dispersed into 9 mL of water under ultra-sonication for 5 min and then 1 mL (from 20 mM) of $AgNO_3$ (2 mM) solution added into solution under continuous stirring 2 h. Finally, the obtained precipitate was centrifuged, washed with distilled and followed by drying at 60 °C, which is used for further experiments and characterization (Scheme: Fig. S1†).

The coating solution was prepared by dispersing 2 mg of catalyst (Ag–PDA@Bi_2O_3) in 1 mL water by ultra-sonication for 5 min. Then, 8 μL of coating solution was drop-coated on SPCE or disk surface of RDSPCE and dried at room temperature. The ring electrode of RDSPCE was modified by 5 μL MnO_2 coating solution prepared by adding 5 mg MnO_2 in 1 mL water and dried at room temperature. The same procedure was followed to prepare Bi_2O_3/SPCE, PDA@Bi_2O_3/SPCE, Ag–PDA/SPCE and Ag–Bi_2O_3/SPCE.

Functionalized PDA was examined by FT-IR (JASCO FT-IR4100, Japan) in the range from 550 to 4000 cm^{-1}. The morphology particle size and lattice fringes were analyzed through High Resolution Transmission Electron Microscopy (HR-TEM) measurements with Surface Area Diffraction Pattern (SAED) (JEM 2010 instrument operating at an accelerating voltage of 200 kV). Dissolved oxygen meter (EUTECH) was used to quantify the amount of oxygen in O_2– and Ar–saturated solution.

Electrochemical experiment was carried out using CHI727e and CHI900 for flow injection analysis work station. Three electrode systems were used for electrochemical work station, catalyst modified electrode as a working electrode, Pt wire as an auxiliary electrode and Ag/AgCl as a reference electrode. Cyclic voltammetry experiment was performed in 0.1 M, pH 7.4 Phosphate Buffer Solution (PBS) at a scan rate of 20 mV s^{-1}. Catalyst-modified glassy carbon rotating disk electrode (GCRDE) was used in O_2-saturated PBS with sweep rate 20 mV s^{-1} in LSV. Flow injection analysis experiment was carried out by our group previously reported RDSPCE cell model.[40] An Ar-saturated PBS was used in FIA, flow rate 0.3 mL min^{-1} and 20 μL of O_2 saturated solution injected into the flow for the H_2O_2 intermediate monitoring.

Results and discussion

Characterization of the Ag-PDA@Bi_2O_3 nanocomposite

The formation of PDA layer on Bi_2O_3 surface was first characterized by FT-IR spectrum. As shown in Fig. 1, compared to those of DA and PDA spectrum, the stretching vibration at 3200—3500 cm^{-1} corresponds to N–H and O–H groups. Whereas, the peak at 1602 and 1497 cm^{-1} corresponds to indole and indoline aromatic ring center, respectively. Finally, the broad peak ranging from 1240 to 1282 cm^{-1} comes from the C–O asymmetric stretching vibration and C–OH asymmetric bending vibration. This is in consistent with previous studies for characterization of PDA thin films deposited by autoxidation of DA.[34,35] The fact that there are no any other extra peaks observed at PDA and PDA@Bi_2O_3 also

confirmed the purity of the as-prepared materials. Overall, melanin like structure PDA layer was strongly formed on the surface of the Bi_2O_3 NPs.[28]

Since we propose to use the Bi_2O_3 NPs as a nanoscale guide for Ag NPs formation, the surface morphology of the catalyst by HR-TEM can provide a direct evidence for such a purpose. At first, as shown in Fig. 2a, a pure nanostructured spherical Bi_2O_3 NPs was observed. Note that the Bi_2O_3 particle formation density was varied at different particle with higher density particle showing very dark and sharp edges and lower density particle of grey color (Fig. S2a†). Simply by mixing the Bi_2O_3 NPs with dopamine solution in Tris-HCl, the polymer matrix was effectively coated on the surface of the Bi_2O_3 NPs, as confirmed from Fig. 2b. Note that this is similar to the polymer matrix layer formed on Bi_2O_3 NPs to that of previously reported PDA layer formation on Fe_3O_4.[36] The polymer coated thickness of PDA was measured as 50 nm. As shown in Fig. 2c, in the absence of PDA, no obvious Ag NPs were observed for the Ag–Bi_2O_3 composites. Yet, small amount of silver layer was found on the edges of Bi_2O_3 surfaces. Note that it could also be visibly observed as yellow color Bi_2O_3 solution turned into slightly whitish yellow while synthesis the composite (Fig. 2c and Fig. S2b†). In other words, the existence of PDA is essential for the successfully loading of large amount of Ag NPs. To prove this, we purposely prepare an Ag–PDA composite *via* $AgNO_3$ solution mixed with PDA powder under stirring condition. As reported earlier, Ag cations can be reduced by PDA powder from metal ions to metal nanoparticles.[26,27,37] As shown in Fig. 2d, large amount of Ag NPs were indeed formed under the PDA condition.

We next improve the preparing method simply by mixing the PDA@Bi_2O_3 with $AgNO_3$. The surface morphology of the as-prepared Ag–PDA@Bi_2O_3 composite was further studied

by HR-TEM. As shown in Fig. 3 and Fig. S3, there is a layer of mixture of Ag film and Ag NPs on the PDA@Bi_2O_3 surface. The Ag NPs was found to form on PDA@Bi_2O_3 surface with spherical shape but in different size. The average particles size of Ag NPs were ~34 nm (Table S1†).[37] Note that higher amount Ag NPs were formed on PDA@Bi_2O_3 surface due to PDA reducing properties.[27,37] The crystal nature of the Ag NPs was studied by SAED image. Figs. 3c and 3d show the lattice fringes and SAED pattern of Ag NPs in Ag–PDA@Bi_2O_3 composite. It is clear that {111}, {220}, {200} lattice plane of face center cubic (fcc) crystal nature of Ag NPs were formed at the Ag-PDA@Bi_2O_3 composite. This is advantageous since the pattern is similar to the Ag NPs added to improve the performance of a zinc oxide nanowire ultraviolet photodetector.[38]

Electrocatalytic activity of the Ag-PDA@Bi_2O_3 composite electrode for ORR

Fig. 4 compares the electrochemical behavior of different composite electrodes towards ORR. As can be seen, in the absence of Ag NPs, both Bi_2O_3 and PDA@Bi_2O_3 electrodes revealed very low catalytic behavior for the reduction of O_2. On the other hand, both Ag NPs on Ag–PDA and Ag layer on Ag–Bi_2O_3 modified electrodes exhibited good electrocatalytic behavior at ~–0.6 V vs. Ag/AgCl.[37] As to the Ag-PDA@Bi_2O_3 composite electrode, a lower reduction potential at –0.38 V with an enhanced catalytic activity in ORR was observed. The observation of a totally different cyclic voltammograms also indicates that there is a synergetic effect among PDA, Ag NPs and Bi_2O_3 enhance the electrocatalytic ability and hence a lower potential for ORR. Compared to those of Ag layer on Bi_2O_3 and Ag NPs on

PDA@Bi_2O_3, the Ag NPs on PDA with Bi_2O_3 supporting substrate improved the catalytic activity with a lower reduction potential for ORR. To elucidate this, the ORR electrocatalytic activity of the Ag–PDA@Bi_2O_3 was investigated more detail in O_2-saturated 0.1 M, pH 7.4 PBS using a rotating disk electrode system to verify whether O_2 is reduced with an n-value of 2 or 4.

We purposely compare different electrochemical behavior of ORR at three representative electrodes of Au–RDE, GC–RDE and Ag–PDA@Bi_2O_3 modified GC-RDE. It is well known that GC electrode catalyzes the ORR with an n-value of 2 and nano–Au electrode involves two step $2e^-$ transfer for ORR and H_2O_2 reduction, respectively. As shown in Fig. 5a, at the Au-RDE, two step $2e^-$ transfer was truly observed at ~–0.37 V for ORR and at –0.7 V for H_2O_2 reduction. The GC-RDE, on the other hand, only shows a $2e^-$ transfer ORR at –0.7 V. It is interesting that the Ag-PDA@Bi_2O_3 modified electrode shows a single and sharp ORR peak at –0.38 V. In order to quantitatively evaluate the ORR kinetics (including n-values), analysis of the RDE data was done using the Koutecky–Levich (K–L) formalism as given by:[20] $1/j = 1/j_k + 1/(B\omega)^{1/2}$, in which $B = 0.62nFC_oD_o^{2/3}/v^{1/6}$ where j is the measured current density, j_k is the kinetic current density, ω is the rotation rate, n is the overall number of electrons transferred in oxygen reduction, F is the Faraday constant (F = 96 485 C mol^{-1}), C_o is the bulk concentration of O_2 (0.25×10^{-3} mol L^{-1}), D_o is the diffusion coefficient of O_2 in the electrolyte (2.51×10^{-5} cm^2 s^{-1}),[6] and v is the viscosity of the electrolyte. Active surface area can be calculated by Randles-Sevcik equation (Fig. S4† and Table S2†). Figs. 5b and 5c show the ORR polarization curve at different rotation rate ranging from 150 to 1000 rpm. The ORR current responses were found to increase with the rotation rate, and this process represented a diffusion control

process. Fig. 5d express the K-L plot via the inverse current density (j^{-1}) as a function of inverse of the square root of the rotation rate. According to the K-L equation (Table S2†), the n of ORR was calculated to be 3.69 at –0.38 V and j_k value of 18.18 mA cm^{-2}. The corresponding K–L curves at various potentials exhibit good linearity, and the slopes remain almost unchanged over the potential range from –0.38 to –0.78 V (Fig. S5†), suggesting that the electron transfer numbers for oxygen reduction at different potentials are similar. The linearity and parallelism of the plots are considered as an indication of first-order reaction kinetics with respect to the concentration of dissolved O_2.[20] This value is good compared to previously reported Ag–based ORR catalyst[10–13,16] and other non-Pt based catalyst.[3,9,19–25,29–31]

Instead of using RDE system, our group previously reported a simple way to identify the $4e^-$ transfer using a flow injection system.[39,40] Fig. S6† illustrates the instrumental setup and the working principle. Note that MnO_2 NPs is a well-known catalyst for H_2O_2 oxidation. As shown in Fig. 6, by injection 20 μL of O_2–sat. solution, the ORR reaction was found to occur at applied potential –0.38 V on the Ag-PDA@Bi_2O_3 modified disk electrode and only little amount of H_2O_2 produced from this reaction was monitored at the MnO_2 NPs modified ring electrode at oxidation potential of 0.8 V.[39] Based on the results, the achievement of $4e^-$ transfer ORR was as high as 98% since only ~2% H_2O_2 oxidation was observed. Note that, by calculating from the H_2O_2 formation percentage, n = 3.92 is a further evidence of $4e^-$ transfer in ORR. Since the Ag–PDA@Bi_2O_3 possessed good electrocatalytic ability towards ORR, its application for use as a sensor for detecting dissolved oxygen was also evaluated.[6,14] Fig. S7† shows voltammetric behavior of dissolved oxygen in Ar-saturated 0.1 M PBS (pH 7.4) and a wide linear range from 0.0841—6.048 mg

L^{-1} with a sensitivity of 2.1 μA mg^{-1} was achieved. It is thus also suitable for application in environmental analysis. Stability is one of the crucial factors in fuel cell and sensor application. The Ag–PDA@Bi_2O_3 composite also showed good stability in O_2-sat. PBS. After 2500 cycles under a scan rate of 200 mV s^{-1}, the maximum current remained similarly except the onset potential shifted positive slightly. This catalyst shows superior stability without any binding material (like Nafion) to modify the electrode due to the superior PDA adhesion properties. Long-term stability of this composite is also excellent to retain 99% of activity towards ORR after 57 days.

Conclusions

In summary, we have demonstrated successful synthesis a simple way of Ag–PDA@Bi_2O_3 nanocomposite with good stability. Face centered cubic lattice crystal nature Ag NPs can be easily formed on the PDA@Bi_2O_3. The Bi_2O_3 NPs helped to enhance the catalytic activity of Ag NPs with a lower potential in $4e^-$ transfer pathway of ORR. Electrocatalytic tests for ORR indicated that the synthesized Ag–PDA@Bi_2O_3 nanocomposite displayed superior activity. The enhanced ORR activity is attributed to the synergistic effects of the composition and dominant face centered cubic lattice crystal nature Ag NPs. This work would be highly impactful in the rational design of future bimetallic alloy nanostructures with high catalytic activity for fuel cell systems.

Acknowledgment

The authors gratefully acknowledge financial support from the Ministry of Science and Technology of Taiwan. The author heartedly acknowledge to Prof. Annamalai Senthil Kumar, Environmental and Analytical Chemistry Division, Vellore Institute of Technology University, Vellore, India and Dr. Ting-Hao Yang, Department of Soil and Environmental Science, National Chung Hsing University, Taichung, Taiwan for given some useful guidance to carry out this work.

Notes

Electronic Supplementary Information (ESI) available. Scheme of the work, preparation of Ag–Bi_2O_3, Ag–PDA, Randles-Sevcik equation for surface area calculation, K-L plot comparison table for n-value calculation, K-L plot diagram of catalyst at different potential, schematic diagram of FIA, oxygen sensor and stability experiment. See DOI:

References

1 S. Guo, S. Zhang and S. Sun, *Angew. Chem. Int. Ed.,* 2013, **52**, 8526.

2 K. B. Liew, W. R. W. Daud, M. Ghasemi, J. X. Leong, S. S. Lim and M. Ismail, *Inter. J. Hyd. Ener.,* 2014, **39**, 4870.

3 T.-H. Yang, S. Venkatesan, C.-H. Lien, J.-L. Chang and J.-M. Zen, *Electrochim. Acta,* 2011**,** **56**, 6205.

4 S. Venkatesan, A. S. Kumar, J.-F. Lee, T.-S. Chan and J.-M. Zen, *Chem. Eur. J.,* 2012, **18**, 6147.

5 K. E. Toghill and R. G. Compton, *Inter. J. Electrochem. Sci.,* 2010, **5**, 1246.

6 C.-C. Yang, A. S. Kumar and J.-M. Zen, *Electroanalysis,* 2006, **18(1)**, 64.

7 X. Ma, H. Meng, M. Cai and P. K., Shen, *J. Am. Chem. Soc.,* 2012, **134**, 1954.

8 F. Han, T. Zhang, J. Yang , Y. Hu and J. Chen, *Adv. Mat.,* 2014, **26**, 2047.

9 H. Wang, X. Bo, A. Wang and L. Guo, *Electrochem. Comm.,* 2013, **36**, 75.

10 L. Tammeveski, H. Erikson, A. Sarapuu, J. Kozlova, P. Ritslaid, V. Sammelselg and K. Tammeveski, *Electrochem. Comm.,* 2012, **20**, 15.

11 C.-L. Lee, H.-P. Chiou, C.-M. Syu and C.-C. Wu, *Electrochem. Comm.,* 2010, **12**, 1609.

12 Y. Lu, Y. Wang and W. Chen, *J. Pow. Sour.,* 2011, **196**, 3033.

13 Y. Lu and W. Chen, *J. Pow Sour.,* 2012, **197**, 107.

14 Y. Zhang, M. Ma and Q. Chen, *J. Appl. Electrochem.,* 2014, **44**, 419.

15 B. B. Blizanac, P. N. Ross and N. M. Markovic, *J. Phys. Chem. B*, 2006, **110**, 4735.

16 P. Singh and D. A. Buttry, *J. Phys. Chem. C*, 2012, **116**, 10656.

17 D. A. Slanac, W. G. Hardin, K. P. Johnston and K. J. Stevenson, *J. Am. Chem. Soc.*, 2012, **134**, 9812.

18 J. Guo, A. Hsu, D. Chu and R. Chen, *J. Phys. Chem. C*, 2010, **114**, 4324.

19 P. Chen, T. Y. Xiao, Y. H. Qian, S. S. Li and S. H. Yu, *Adv. Mat.,* 2013, **25**, 3192.

20 R. Liu, D. Wu, X. Feng and K. Mullen, *Angew. Chem.,* 2010, **122**, 2619.

21 I. Y. Jeon, S. Zhang, L. Zhang, H. J. Choi, J. M. Seo, Z. Xia, L. Dai and J. B. Baek, *Adv. Mat.,* 2013, **25**, 6138.

22 Z. Yang, Z. Yao, G. Li, G. Fang, H. Nie, Z. Liu, X. Zhou, X. Chen and S. Huang, *ACS Nano,* 2012, **6**, 205.

23 Z. W. Liu, F. Peng, H. J. Wang, H. Yu, W. X. Zheng and J. Yang, *Angew. Chem. Int. Ed.,* 2011, **50**, 3257.

24 L. Yang, S. Jiang, Y. Zhao, L. Zhu, S. Chen, X. Wang, Q. Wu, J. Ma, Y. Ma and Z. Hu, *Angew. Chem. Int. Ed.,* 2011, **50**, 7132.

25 C. Zhang, N. Mahmood, H. Yin, F. Liu and Y. Hou, *Adv. Mat.,* 2013, **25(35)**, 4932.

26 H. Lee, S. M. Dellatore, W. M. Miller and P. B. Messersmith, *Science,* 2007, **318**, 426.

27 Y. Liu, K. Ai and L. Lu, *Chem. Rev.,* 2014, **114**, 5057.

28 K. Ai, Y. Liu, L. RuanLu and G. M. Lu, *Adv. Mat.,* 2013, **25**, 998.

29 W. Wei, H. Liang, K. Parvez, X. Zhuang, X. Feng and K. Mullen, *Angew. Chem. Int. Ed.* 2014, **53**, 1570.

30 K. E. Lee and B.-S. Kim, *J. Mat. Chem., A* 2014, **2**, 6167.

31 S. M. Sayed and K. Juttner, *Electrochem. Acta,* 1983, **28**, 1635.

32 C. Jeyabharathi, J. Mathiyarasu and K. L. N. Phani, *J. Appl. Electrochem.,* 2009, **39**, 45.

33 I. Arul Raj and K. I. Vasu, *J. Appl. Electrochem.,* 1993, **23**, 728.

34 R. A. Zangmeister, T. A. Morris and M. J. Tarlov, *Langmuir,* 2013, **29**, 8619.

35 S. Yu, Y. Chen, H. Li, L. Yang, Y. Chen and Y. Yin, *J. Mol. Str.,* 2010, **982**, 152.

36 Y. Xie, B. Yan, H. Xu, J. Chen, Q. Liu, Y. Deng and H. Zeng, *ACS Appl. Mat. & Inter.,* 2014, **6**, 8845.

37 F. Wang, R. Han, G. Liu, H. Chen, T. Ren, H. Yang and Y. Wena, *J. Electroanal. Chem.,* 2013, **706**, 102.

38 S.-K. Tzeng, M.-H. Hon and I.-C. Leuc, *J. Electrochem. Soc.*, 2012, **159**, H440.

39 A. S. Kumar, S. Sornambikai, S. Venkatesan, J.-L. Chang and J.-M. Zen, *J. Electrochem. Soc.,* 2012, **159**, G137.

40 T.-H. Yang, C.-Y. Liao, J.-L. Chang, C.-H. Lien and J.-M. Zen, *Electroanalysis,* 2009, **21**, 2390.

299 **Figure 1**

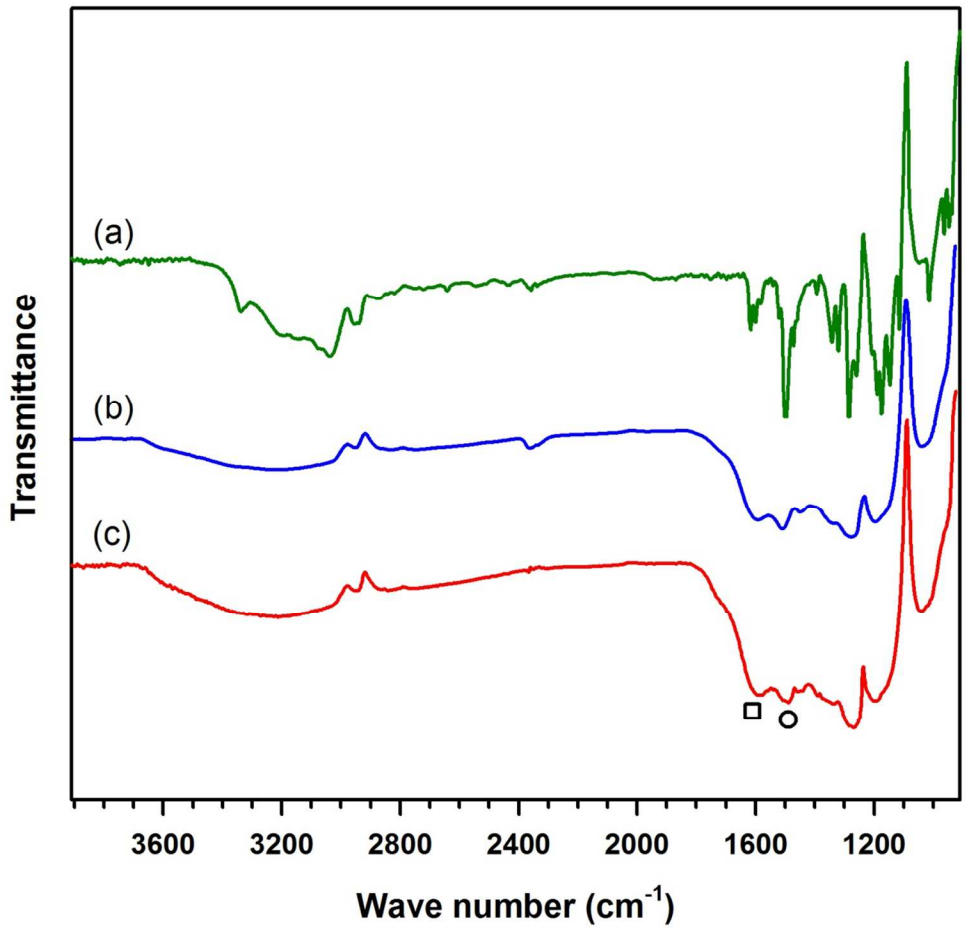

300

301

302 Fig. 1 Characterization of DA (a), PDA (b) and PDA@Bi_2O_3 (c) by FT-IR

303 spectroscopy.

304 **Figure 2**

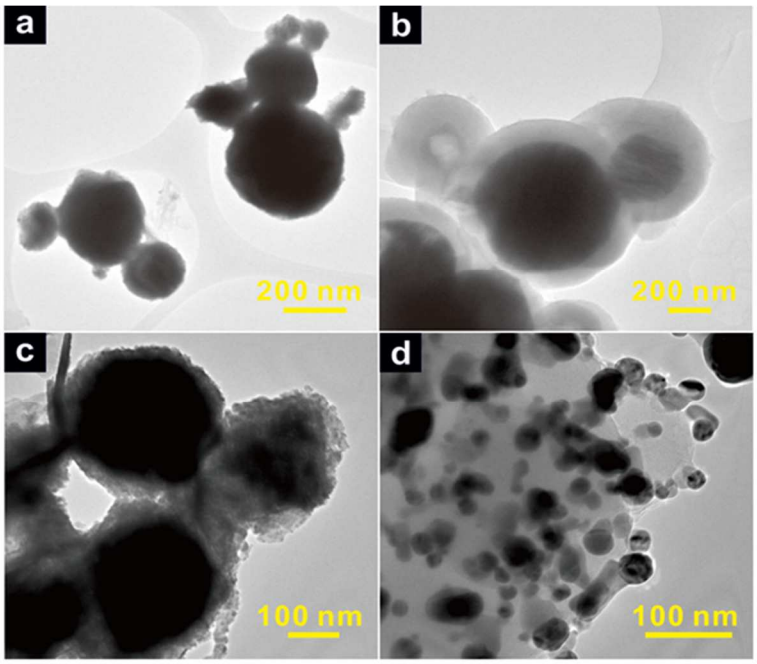

305

306 Fig. 2 HR-TEM images of Bi_2O_3 (a), PDA@Bi_2O_3 (b), Ag-Bi_2O_3 (c) and Ag-PDA (d).

307 **Figure 3**

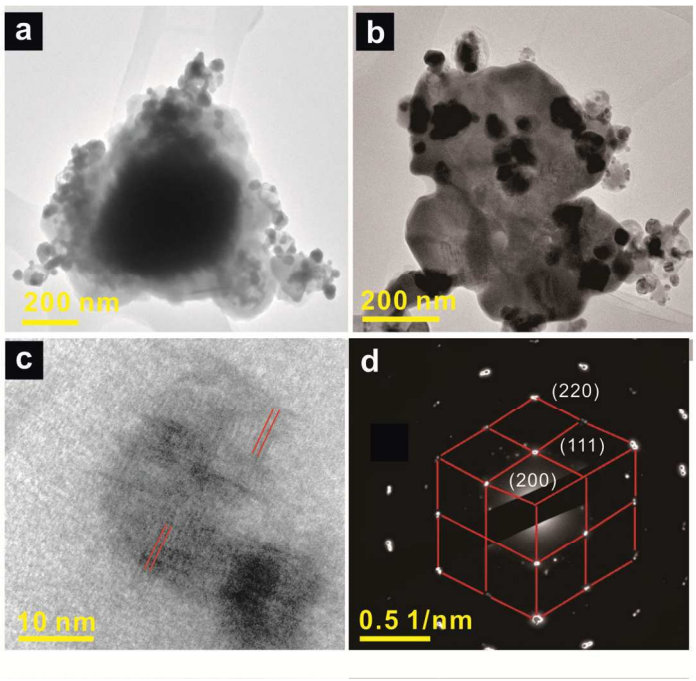

308

309 Fig. 3 HR-TEM images of Ag-PDA@Bi_2O_3 (a), (b) and lattice fringes of silver in Ag-

310 PDA@Bi_2O_3 (c) and SAED image for crystal nature characterization of Ag NPs in Ag-

311 PDA@Bi_2O_3 (d).

312

313

314

315

316

317

318 **Figure 4**

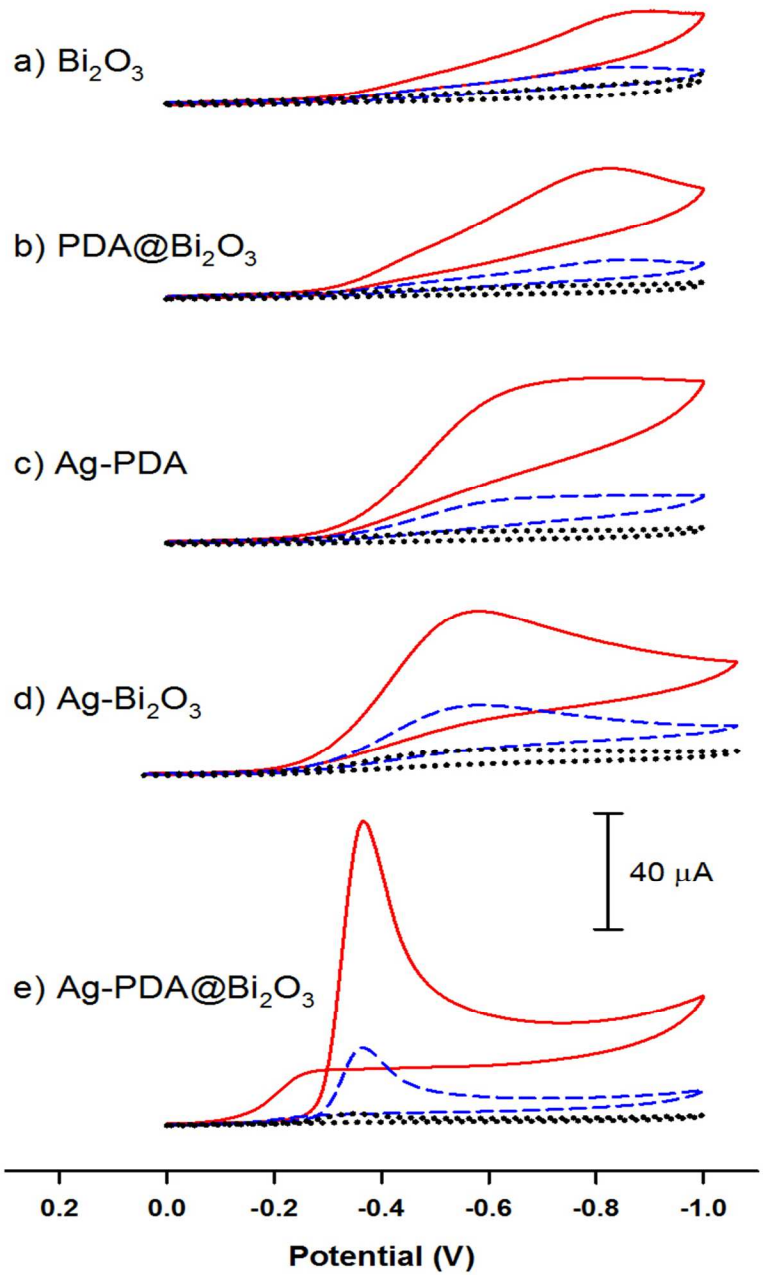

319

320 Fig. 4 Cyclic voltammograms of different composite-modified SPCE for ORR in
321 atmospheric (dashed line), anaerobic (dotted line) and O_2-saturated (solid line) PBS
322 (pH = 7.4), respectively.

323 **Figure 5**

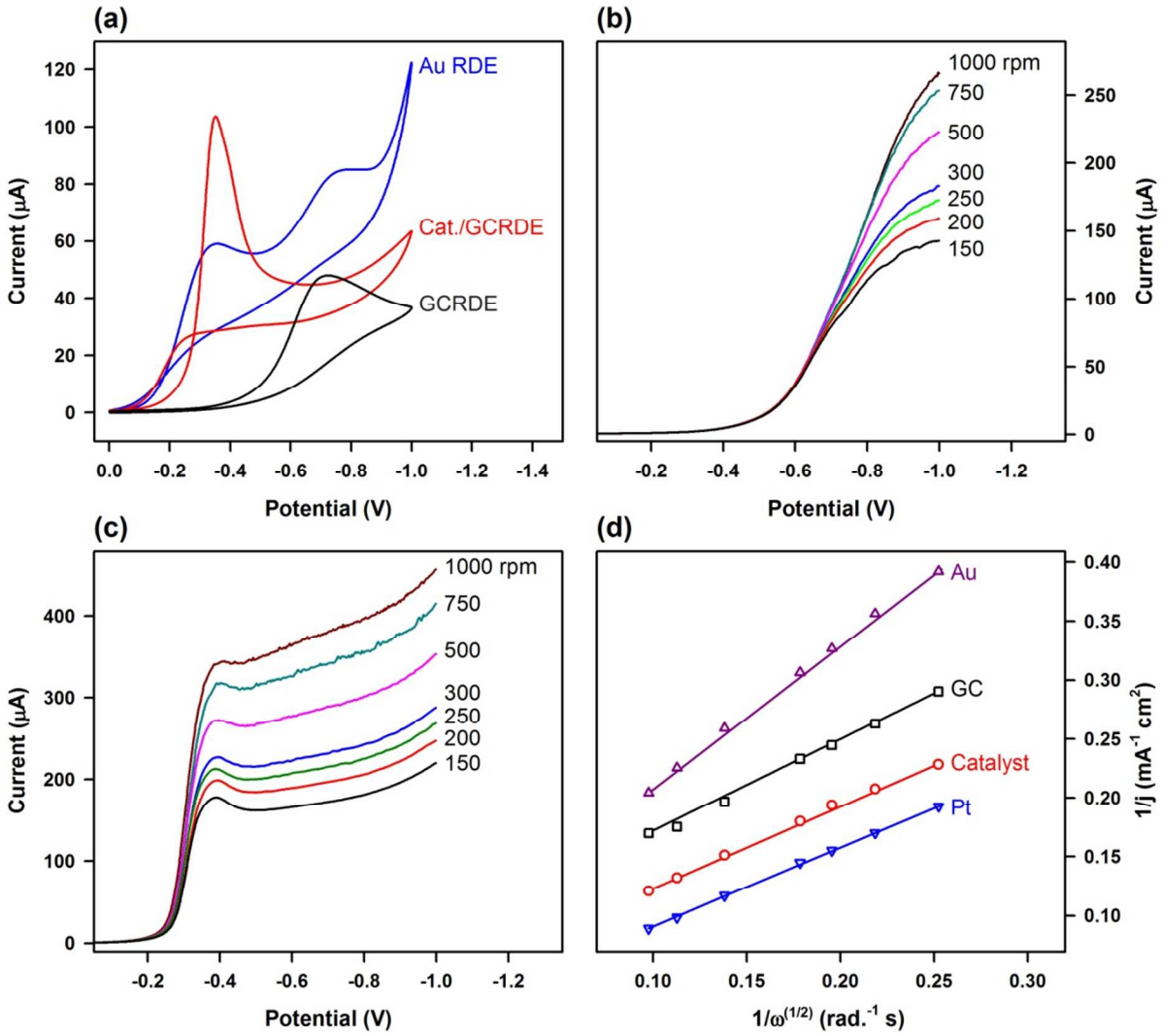

324

325 Fig. 5 (a) Cyclic voltammograms for ORR at different RDEs. RDE voltammetry curve
326 for ORR on GCRDE (b) and Ag-PDA@Bi_2O_3-modified GCRDE (c) in 0.1 M O_2-
327 saturated PBS (pH 7.4) at various rotation rates. (c) RDE diffusion curve of different
328 electrodes (GC at –0.9 V, Ag-PDA@Bi_2O_3 at –0.38 V). (d) K-L plots.

329 **Figure 6**

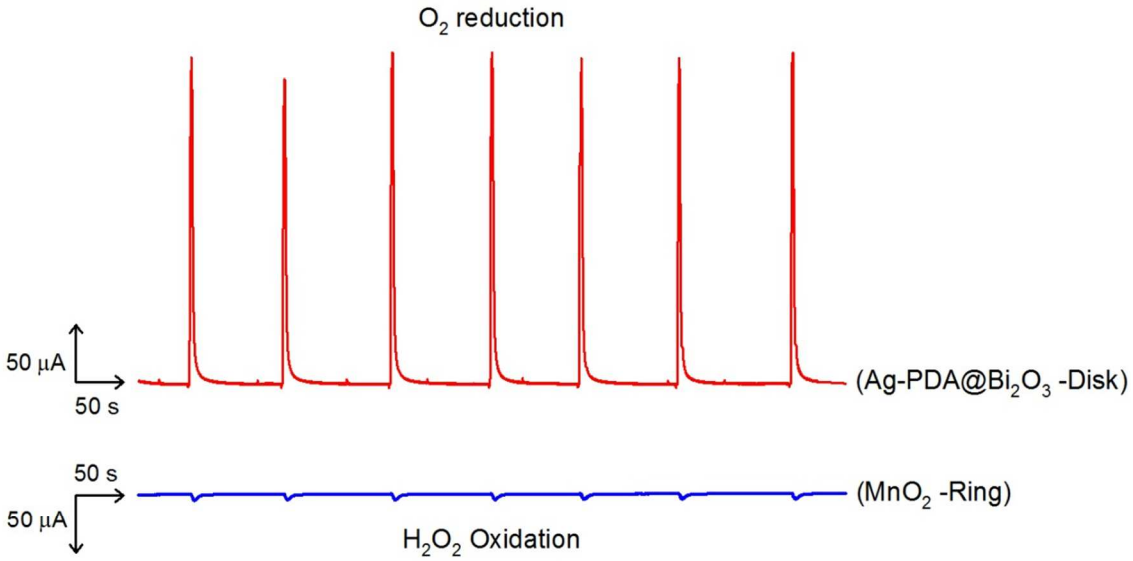

330

331 Fig. 6 Flow injection Analysis of H_2O_2 oxidation on nano MnO_2 catalyst on ring at an
332 operating potential 0.8 V vs. Ag/AgCl and ORR on Ag-PDA@Bi_2O_3 catalyst coated on
333 disk at detection potential –0.38 V vs. Ag/AgCl with flow rate 0.4 mL min^{-1}.

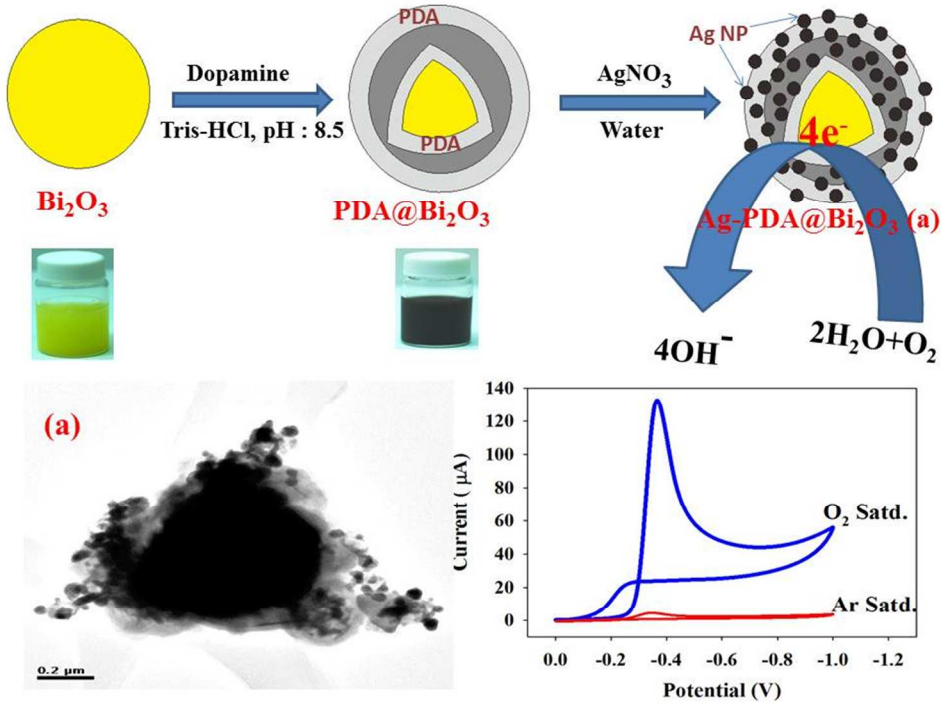

334

335 Graphic abstract